Wideband Mechanism Model and Parameter Extracting for High-Power High-Voltage High-Frequency Transformers

Chen Liu, Lei Qi, Xiang Cui, *Senior Member, IEEE*, Zhiyuan Shen, and Xiaoguang Wei

***Abstract*—The high-power high-voltage high-frequency transformer (H^3T) is a key equipment to develop the isolated high-power dc–dc converter. In this paper, a wideband mechanism model is proposed to analyze the external behaviors of the H^3T. This model is characterized by elaborate considerations on magnetic and capacitive effects of the H^3T, including electrostatic couplings between windings, magnetic core, and the enclosure, with parameters which have explicit physical meanings. In terms of large number of turns and racetrack windings of the H^3T, a finite-element method based on weighted algorithm is used to extract model inductance and capacitance parameters. To verify the proposed model and corresponding parameter extraction method, impedance characteristics of an H^3T prototype under open circuit, short circuit, and load conditions are measured and simulated over a wide frequency band. The results show that the proposed model is valid up to 300 kHz. Besides, when one or two windings of the H^3T are grounded, the proposed model may be reduced to traditional six or three capacitance models due to changes of winding-to-ground capacitances, which may account for shift of resonant frequencies. The proposed model and corresponding analyses are helpful to electromagnetic design and external behavior investigations of the H^3T.**

***Index Terms*—Finite-element method, grounding, high-frequency (HF) transformers, modeling.**

I. Introduction

RECENTLY, as the demand for integrating large-scaled offshore windfarms and new direct current (dc) sources (including fuel cells, photovoltaics, batteries, redox flow photovoltaics, etc.) increases; the investigations on establishing dc networks have gained widespread attention [1]–[4]. The high-power dc–dc converter with intermediate high-frequency (HF) transformers is the key equipment to develop dc networks as it can achieve large scale of dc transmission and flexible control, while guaranteeing the bilateral galvanic isolation. Besides, with the increased operating frequency, volume and weight of the transformer will be significantly reduced. Some kilowatt-scaled HF transformers applying to dc–dc converters have been developed in the laboratory [5]–[9], but HF transformers with higher power which applied to megawatt-scaled HVDC applications still stay at concepts stage [2]–[4]. The strategy of multiple transformers in series or parallel has been researched in [7]–[9] to meet power requirements. However, as the number of transformers increases, this strategy may be at risk of low reliability and high circulating current losses. Therefore, it is necessary to enhance the power and voltage level of a single HF transformer.

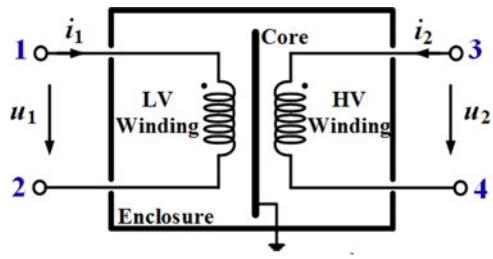

Fig. 1. Schematic diagram of a H^3T.

A schematic diagram of a high-power high-voltage high-frequency transformer (H^3T) is shown in Fig. 1. As operating frequency increases, parasitic capacitances, which are closely related to physical structure of the transformer, are not neglected and become main factors to impact normal operating performance of the transformer and the interaction with power electronics devices at its sides [10], [11]. Therefore, traditional transformer models in low frequency may not be applied to this subject as they fail to include capacitive effects of the H^3T. As power and voltage increase, the number of turns may be very large, and an oil-immersed transformer with an enclosure may be employed to guarantee the sufficient dielectric strength for megawatt power application. Furthermore, traditional magnetic material used as a core of low-power HF transformers, such as ferrite, may be not suitable for the H^3T due to its low-saturation flux density and poor mechanical strength [6]. Instead, metal soft magnetic material, such as nanocrystalline, which has lower loss density, higher saturation flux density, and stronger mechanical strength may be used as a magnetic core of the H^3T [5], [6], [25]. Different from a ferrite core which may be taken as an insulator, the metallic core should be taken as a conductor as the resistivity of those materials are only about 100 times larger than copper. As a result, the metallic core of the H^3T has to be connected to the enclosure and grounded, just like traditional power transformers with silicon-steel plate cores. Otherwise,

Manuscript received February 16, 2015; accepted July 27, 2015. Date of publication August 5, 2015; date of current version December 10, 2015. This work was supported in part by the National High Technology Research and Development of China (863 Program) under Grant 2012AA050401, by the National Natural Science Foundation of China under Grant 51277065, and by the Chinese Universities Scientific Fund under Grant 2015XS11. Recommended for publication by Associate Editor J. Biela.

C. Liu, L. Qi, X. Cui, and Z. Shen are with the State Key Laboratory for Alternate Electrical Power System with Renewable Energy Sources, North China Electric Power University, Beijing 102206, China (e-mail: qilei@ncepu.edu.cn; liuchen12315@ncepu.edu.cn; x.cui@ncepu.edu.cn; dragonszy@163.com).

X. Wei is with the State Grid Smart Grid Research Institute, Beijing 100192, China (e-mail: weixiaoguang@sgri.sgcc.com.cn).

Color versions of one or more of the figures in this paper are available online at http://ieeexplore.ieee.org.

Digital Object Identifier 10.1109/TPEL.2015.2464722

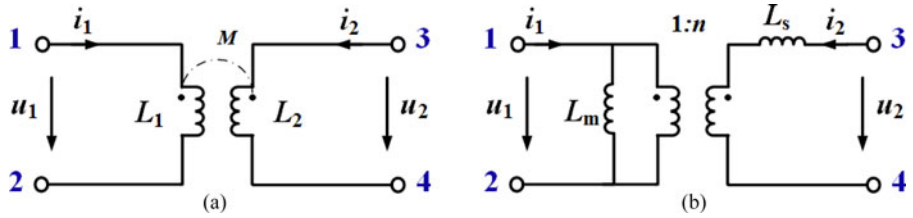

Fig. 2. Lossless magnetic model. (a) Coupled inductors model. (b) Equivalent model using an ideal transformer.

the floating potential of the metallic core and enclosure may cause discharge to the ground and harm insulations of the H^{3}T. As a result, the capacitive effects between windings, magnetic core, and enclosure of the transformer should be elaborately considered in the H^{3}Ts. In addition, cross section of the metallic core is often rectangular as these materials are tape wound, maybe resulting in racetrack windings of the H^{3}T [5], [6]. For the windings, the finite-element method (FEM) in case of two-dimensional axial symmetry is not used directly as well.

As is well known, the low-frequency characteristics of a transformer mainly depend on magnetic couplings, on which there have been extensive studies [12]–[17]. Recently, HF models are turned to be the focus of research. The refined models considering distributed parameters of every single turn have been developed to research transient behavior of power frequency transformers [18], [19]. Relevant methods may be used to analyze the H^{3}Ts. However, considering a large number of turns, these models will contain thousands of circuit components which are too complicated to investigate the external behavior of the transformers. Besides, the black-box models based on experimental measurement have been proposed without having to know the inner structure of a transformer [10], [20], [21]. However, these models fail to link internal geometry and external behavior of the transformer and cannot be applied to the design of H^{3}T. The equivalent circuit models focusing on winding level have been proposed in [11], [22]–[24], where the transformer windings were equivalent as several lumped parameters based on analytical or numerical methods, which are convenient to analyze steady-state behavior of HF transformers. However, these models are mainly applied to low-power HF transformer without enclosure, and the magnetic core is usually an insulator due to the use of ferrite. As a result, for the H^{3}T, electrostatic couplings between windings, magnetic core, and enclosure could not be satisfactorily considered with these models. Furthermore, these models are all focused on transformers with axial symmetric windings. As a result, their parameter extraction methods may not be applied to the H^{3}Ts.

In summary, existing models may not satisfy the demands for analyzing external behavior and designing of the H^{3}T, and there are few corresponding methods to extract model parameters. In this paper, a wideband mechanism model for the H^{3}T is proposed, where the magnetic and electrostatic effects of the transformer are fully considered with parameters having explicit physical meanings. In terms of racetrack windings and large number of turns of a 30 kW, a 20-kHz H^{3}T prototype in the laboratory, an FEM based on weighted algorithm is proposed to extract inductance and capacitance parameters of the model. By impedance measurements of the prototype under open circuit, short circuit, and load conditions over a wide frequency band, the proposed model and its parameter extracting method are proved to be valid up to 300 kHz. Besides, the validity of the proposed model when different windings of the H^{3}T are grounded is discussed and verified, and the relationships between the proposed model and traditional six and three capacitance models are revealed.

II. Wideband Mechanism Model

Electric behavior of the H^{3}T at low frequency is mainly due to the magnetic couplings between windings, while electrostatic couplings between windings, magnetic core, and enclosure of the transformer should not be ignored at HF. Therefore, detailed analyses on magnetic and electrostatic couplings of the H^{3}T are necessary to establish the wideband model.

A. Magnetic Mechanism Model

As we focus on external behaviors of the HF transformers, the magnetic core is considered working in linear region. Therefore, consider the classical coupled inductors model as shown in Fig. 2(a). The inductance matrix is fully determined by the self- and mutual inductances, and the leakage inductance seen from the secondary side 3–4 in Fig. 2(a) is

$$L_s = L_2 - M^2/L_1 = \left(1 - k^2\right) L_2 \tag{1}$$

where k represents the coupling coefficient. In H^{3}T, k is usually near to unity due to the use of metallic magnetic core. As a result, (1) may lead to inaccurate determination of L_s as it is represented by the difference of two terms which are very close to each other [12]. Considering that the leakage inductance is a key parameter which affects the impedance characteristics of the HF transformer [20], [21], an equivalent model using an ideal transformer is employed in this paper. As shown in Fig. 2(b), L_m is the core inductance seen from the primary side 1–2, and n is turn ratio of the ideal transformer

$$L_m = L_1, \quad n = k\sqrt{\frac{L_2}{L_1}}. \tag{2}$$

The equivalence of the two models may be verified by using Kirchhoff Current Law at the primary side and Kirchhoff Voltage Law at the secondary side [13]. By using an ideal transformer, the leakage inductance in the equivalent model appears as an independent parameter and it may be directly calculated through the analysis of the magnetic field. Furthermore, the

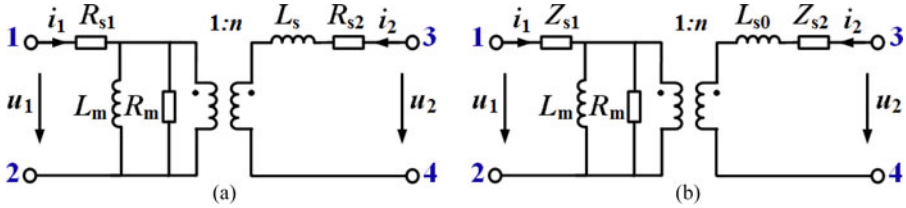

Fig. 3. Loss magnetic model. (a) Traditional low frequency model. (b) Model including frequency-dependent winding parameters.

mutual inductance is removed in this model which makes the model more suitable for the circuit analysis.

For a real transformer, the losses of the windings and core should be considered to get an accurate model. By adding two winding resistances (R_{s1} and R_{s2}) in series with the leakage branch and a core loss equivalent resistance (R_m) in parallel with the magnetizing branch, a loss magnetic model is obtained as shown in Fig. 3(a). Obviously, this is a traditional transformer model at low frequency, which is widely used in power system and electrical machinery applications [13]. Considering that winding resistances and internal inductances will be functions of frequency due to eddy current effects, they are incorporated and represented as winding internal impedances, i.e., Z_{s1} and Z_{s2}. Besides, the external inductance of the windings, which may be taken as frequency independent if the proximity effect is ignored [13], is represented as L_{s0} referred to the secondary side. The final magnetic model is shown in Fig. 3(b). However, this model is still not suitable to research wideband external behaviors of the H^{3}T because it fails to consider capacitive effects between windings, magnetic core, and the enclosure.

B. Capacitive Mechanism Model

It has become widely aware that stray capacitances are related to electrostatic couplings between conductors in the transformer. As illustrated in Fig. 1, the conductors in the H^{3}T mainly include the LV winding conductors, the HV winding conductors, and the grounding magnetic core connected to enclosure of the transformer. As a voltage drop occurs across each conductor of the transformer, the capacitances must exist between these conductors, including the core and enclosure.

Considering voltages of the primary winding, the secondary winding and between the two windings (u_1, u_2, and u_0), a two winding transformer may be taken as a three input multipole, and the electrostatic effects of the windings could be modeled by a six-capacitance model as shown in Fig. 4 focusing on the winding level [11], [20]–[24]. This six-capacitance model is suitable for low-power HF transformers whose magnetic core is usually ferrite and may be regarded as an insulator. However, in the H^{3}T, the metallic core connected to the enclosure is a conductor and has to be grounded in order to avoid discharge to the ground. Therefore, electrostatic couplings of the H^{3}T cannot be fully considered with traditional six-capacitance model as the capacitances between windings, magnetic core, and enclosure are reduced.

For improving the model in Fig. 4, a more complete capacitive model for the H^{3}T including all electrostatic couplings is

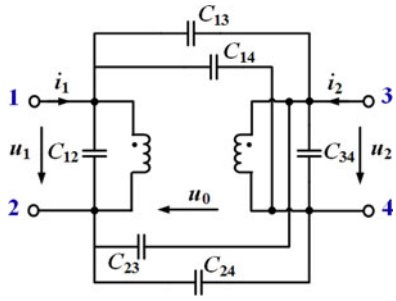

Fig. 4. Six-capacitance equivalent model.

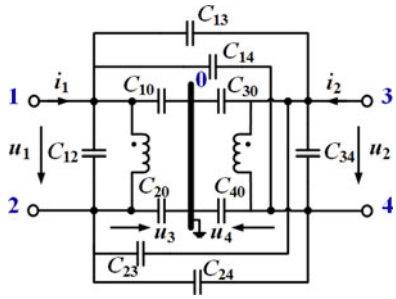

Fig. 5. New capacitive model.

proposed in this paper. As shown in Fig. 5, the primary and secondary windings are represented as electrodes 1, 2 and 3, 4, respectively, and particularly the grounded magnetic core connected to the enclosure is represented as the grounding electrode 0. The self-capacitances of the primary and secondary winding are represented as C_{12} and C_{34}, respectively, and the capacitances between the primary and secondary winding are represented as C_{13}, C_{24}, C_{14}, and C_{23}. Especially, except for the six capacitances which account for electrostatic effects of the windings, four new capacitances, i.e., C_{10}, C_{20}, C_{30}, and C_{40}, are added between winding terminals and the ground to account for capacitive effects between windings, magnetic core, and enclosure of the H^{3}T.

In this new capacitive model, electrostatic effects between electrodes of the H^{3}T are fully considered with ten capacitance parameters, which are only determined by geometry, size, and mutual alignment of the conductors and permittivity of the dielectrics. These capacitance parameters may be extracted by a two-dimensional (2-D) FEM based on weighted algorithm which will be presented in Section III. Besides, the relationships between the proposed new model and traditional capacitive models will be discussed in Section V.

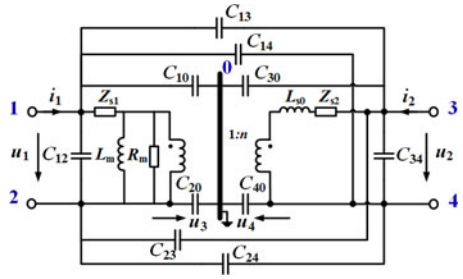

Fig. 6. Wideband mechanism model of the H^{3}T.

Combining the magnetic and capacitive model of the H^{3}T, the wideband model is proposed as shown in Fig. 6. In the proposed wideband model, magnetic and capacitive effects of the H^{3}T are fully considered, including the electrostatic couplings between windings, magnetic core, and enclosure of the transformer. Furthermore, with the proposed model, rigorous mechanism links between *R*, *L*, *C* parameters and physical properties of the H^{3}T are established, and each parameter of the model has explicitly physical meaning. Therefore, the proposed wideband model may be taken as a "mechanism model."

III. Parameters Extraction

Parameters of the wideband mechanism model, as an application of the model, are extracted through a 20-kHz H^{3}T prototype. Photo and 2-D schematic diagram of the prototype are shown in Fig. 7(a) and (b). Main parameters of this prototype are shown in Table I. In this prototype, the LV winding has 12 turns, using rectangular copper wires and with glass fiber for insulation. The HV winding has 1096 turns, using triple-insulated-layers wires (TILW). The core is formed with a pair of U-cores made of the FT-3M nanocrystalline material. Main characteristics of the nanocrystalline core may be found in [5] and [25]. The oil-paper insulation coordination is adopted as the all insulation of the prototype.

A. Inductance and Resistance Parameters

Considering complicated structure of the H^{3}T, the FEM is employed to extract the inductance parameters in order to improve the accuracy. The core inductance L_m is evaluated by magnetostatic field computation [15]. External inductance L_{s0} is evaluated by the leakage magnetic field computation when ampere-turns are compensated, and the complementary variational principle is employed to increase the calculation accuracy [16]. Internal impedances of the windings, i.e., Z_{s1} and Z_{s2}, are calculated by numerical and analytical method taking account of HF effects [13], [26]. Additionally, the core loss equivalent resistance R_m is obtained by the modulus of open-circuit impedance of the transformer at the first resonant frequency, shown as f_1 of Z_{1oc} in Fig. 11.

It has been reported that the contribution of HF effects to impedance of the inductor will decrease with increasing fill factor [14]. Considering that the H^{3}T always has a very large fill factor (0.85 for the prototype) for its high power, the impacts of HF effects on winding impedance of the prototype may be ignored. Accordingly, winding impedances of the prototype including and not including HF effects, i.e., Z_0 and Z_f, are calculated respectively when the HV winding is short circuit. The results are referred to HV winding and shown in Fig. 8. It may be found that there is almost no difference between the value of Z_0 and Z_f. Therefore, it is reasonable to ignore HF effects and take winding resistances and internal inductances as constants in the magnetic model of this prototype. The results of L_m, L_{s0}, R_m, Z_{s1}, and Z_{s2} are given in Table II.

B. Capacitance Parameters

The electrostatic energy stored in the proposed capacitive model shown in Fig. 5 may be calculated as follows:

$$W = \frac{1}{2}u^T C u \tag{3}$$

where *u* is the voltage column vector and *C* is capacitance matrix of the model. Expanding (3) as follows:

$$\begin{aligned} W = {} & \frac{1}{2}(C_{10}+C_{12}+C_{13}+C_{14})u_1^2 \\ & + \frac{1}{2}(C_{13}+C_{23}+C_{30}+C_{34})u_2^2 \\ & + \frac{1}{2}(C_{10}+C_{20}+C_{13}+C_{24}+C_{14}+C_{23})u_3^2 \\ & + \frac{1}{2}(C_{30}+C_{40}+C_{13}+C_{24}+C_{14}+C_{23})u_4^2 \\ & - C_{13}u_1u_2+(C_{10}+C_{13}+C_{14})\,u_1u_3-(C_{13}+C_{14})\,u_1u_4 \\ & - (C_{13}+C_{23})\,u_2u_3+(C_{13}+C_{32}+C_{30})\,u_2u_4 \\ & - (C_{13}+C_{24}+C_{14}+C_{23})\,u_3u_4 = W_1+W_2+W_3+W_4 \\ & + W_{12}+W_{13}+W_{14}+W_{23}+W_{24}+W_{34}. \end{aligned} \tag{4}$$

The total electrostatic energy stored in the prototype is represented as the sum of ten energy terms, i.e., $W_1, W_2, \ldots, W_{34}$, which are determined by the capacitance parameters and applied voltages as shown in Fig. 5. Applying voltages u_1, u_2, u_3, u_4 between corresponding electrodes of the proposed model, each energy term in (4) may be obtained and the capacitance parameters will be extracted. Considering that the capacitance parameters in the proposed model are only determined by physical characteristics of the prototype and are irrelevant to the potential of each electrode, there are no limitations on the values of u_1, u_2, u_3, and u_4.

First, apply u_i to corresponding port while keeping all other ports open circuit, and the total energy *W* will satisfy

$$W\Big|_{k\neq i}^{u_k=0} = W_i\ (i=1,2,3,4)\,. \tag{5}$$

Afterward, apply u_i and u_j to corresponding ports simultaneously while keeping all other ports open circuit, and we have

$$W\Big|_{k\neq i,j}^{u_k=0} = W_{ij}+W_i+W_j \quad (i,j=1,2,3,4 \ \text{ and } \ i\neq j)\,. \tag{6}$$

Take the computation of W_{12} as an example. Applying u_1 and u_2 to the LV and HV winding respectively while keeping

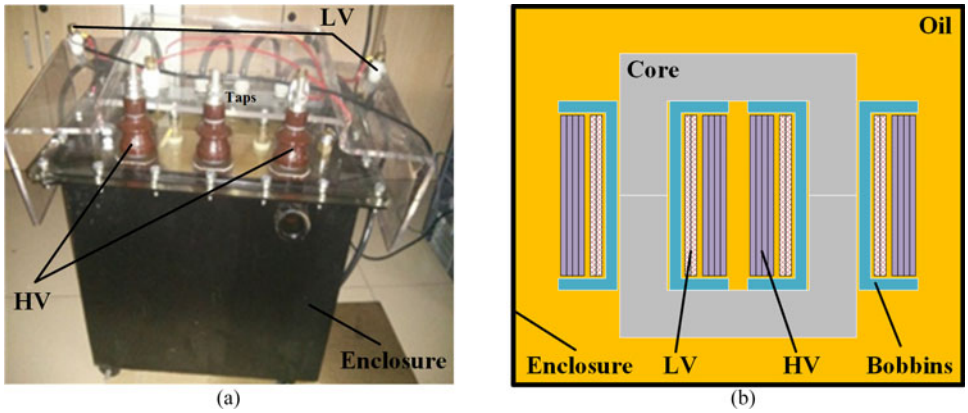

Fig. 7. H^3T prototype used in this paper. (a) Photo. (b) 2-D schematic diagram of the prototype.

TABLE I
MAIN PARAMETERS OF THE PROTOTYPE

Operating frequency	20 kHz
Power rating	30 kVA
Ratio	1:91.3
Core	Nanocrystalline (FT-3M) U150/120/70
Low voltage winding	0.7 kV 12 turns 0.8*36 mm rectangular copper wire
High voltage winding	64 kV 1096 turns 0.5/0.73 mm (inner/outer diameter) TILW

TABLE II
INDUCTANCE AND RESISTANCE PARAMETERS OF THE TRANSFORMER

$L_{\rm m}$ (mH)	L_{s0} (mH)	R_m (Ω)	Z_{s1} (mΩ)	Z_{s2} (Ω)
4.587	42.45	422.8	3.54+$j\Omega$0.158e-3	37.8+$j\Omega$21.5e-6

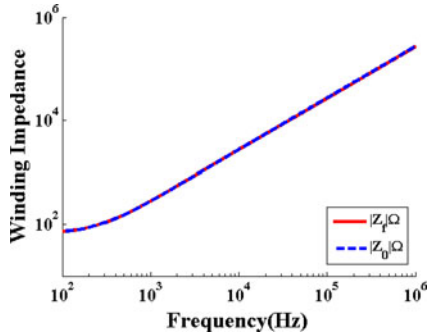

Fig. 8. Comparison of calculated winding impedances including high frequency effect (Z_f) and not including high frequency effect (Z_0).

electrodes 3 and 4 grounding ($u_3 = 0$, $u_4 = 0$), the total energy stored in the transformer will be

$$W\,|_{u_3,u_4=0} = W_{12} + W_1 + W_2.$$

As W_1 and W_2 have been calculated in the first step, then

$$W_{12} = W\,|_{u_3,u_4=0} - W_1 - W_2 = -C_{13}u_1u_2 \Rightarrow C_{13}.$$

Other capacitance parameters may be calculated by similar process. Therefore, calculating total electrostatic energy stored in the transformer is the key to extract the capacitance parameters of the model. Three-dimensional (3-D) FEM may be used to calculate the electrostatic energy. However, the large number of conductors in the prototype will make high computational cost. As an engineering approach, 2-D FEM is employed to extract capacitance parameters as well.

The 3-D schematic diagram of the prototype is shown in Fig. 9(a). Taking axial direction of the winding as *Z*-direction, the cross section of the prototype is shown in Fig. 9(b). It may be seen that winding configuration of the prototype is race-track, which indicates that the 2-D FEM based on axisymmetric structure of the transformer used in [22]–[24] is not feasible. Therefore, a 2-D FEM based on weighted algorithm is proposed in this paper to extract the capacitance parameters of the model.

The electrostatic energies of the prototype are distributed in insulating mediums, which may be classified as conductor insulation of the LV and HV windings, layer insulation inner windings, bobbins, and oil. Numbering these insulating mediums from 1 to 5, and the total electrostatic energy of the prototype may be calculated as follows:

$$W = \sum_{i=1}^{5} \left[W^i_{\rm XOZ} l^i_y + (W^i_{\rm YOZ} + W^i_{\rm YO'Z}) l^i_x\right]. \tag{7}$$

For insulation medium *i*, $Wi_{\rm XOZ}$, $Wi_{\rm YOZ}$, and $Wi_{\rm YO'Z}$ represent its electrostatic energy densities in XOZ, YOZ, and YO′Z sections, respectively, which may be calculated by 2-D FEM based on electrostatic field. On the other hand, l^i_X and l^i_y represent weighted path lengths of insulation medium *i* along *X*- and *Y*-directions, respectively. For the conductor insulation of the LV and HV windings, layer insulation inner windings and bobbins, their weighted path lengths are easy to determine as they are placed around the windings and have explicit lengths in *X*- and *Y*-directions. However, as oil is full inside the

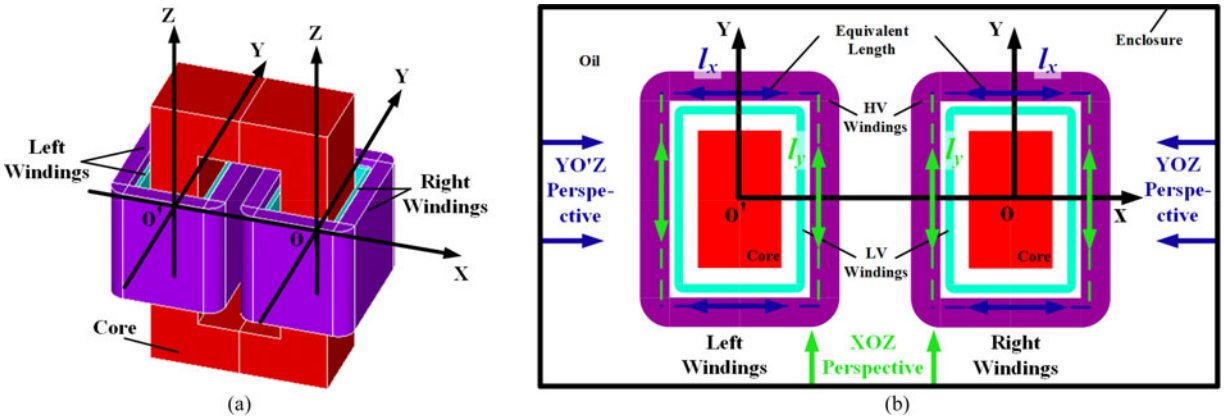

Fig. 9. Schematic diagram of the prototype. (a) 3-D schematic diagram of the prototype. (b) Cross-section of the prototype.

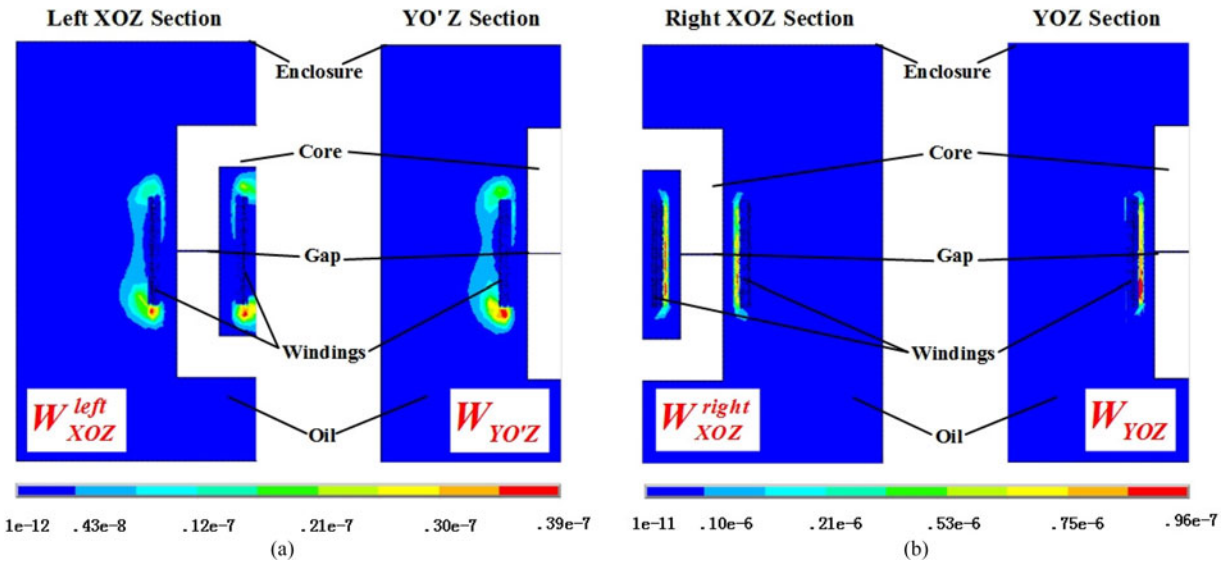

Fig. 10. Electrostatic energy computed results. (a) Left windings. (b) Right windings.

prototype, its weighted path length seems to be hardly confirmed. Fortunately, results of an FEM analysis show that electrostatic energy of oil mainly centralizes between the LV and HV windings. Fig. 10 shows the energy distribution when calculating W_{12}, for example. Therefore, the equivalent length between the LV and HV winding is taken as weighted path length of oil.

With (7), it may be found that to calculate total electrostatic energy stored in the H^{3}T with racetrack windings, three sections of the transformer (XOZ, YOZ, and YO′Z) are needed to be considered. Noticing that in the left windings in Fig. 10(a), electrostatic energy distributions in the XOZ section ($W^{\text{left}}_{\text{XOZ}}$) and YO′Z section ($W_{\text{YO}'\text{Z}}$) are similar. So are $W^{\text{right}}_{\text{XOZ}}$ and W_{YOZ} in Fig. 10(b). Therefore, below equations may be true

$$W^{i(\text{left})}_{\text{XOZ}} = W^{i}_{\text{YO}'\text{Z}}, \quad W^{i(\text{right})}_{\text{XOZ}} = W^{i}_{\text{YOZ}}. \tag{8}$$

Combining (7) and (8), it may be feasible to calculate the total electrostatic energy stored in the transformer only with XOZ section as follows:

$$\begin{aligned} W &= \sum_{i=1}^{5} W^{i}_{\text{XOZ}} l^{i}_{y} + (W^{i(\text{left})}_{\text{XOZ}} + W^{i(\text{right})}_{\text{XOZ}}) l^{i}_{x} \\ &= \sum_{i=1}^{5} W^{i}_{\text{XOZ}} (l^{i}_{x} + l^{i}_{y}). \end{aligned} \tag{9}$$

Table III shows the computed results of capacitance parameters based on (7) and (9), respectively, where the third row shows the relative errors between using the two equations. A good agreement between the results is observed and the deviations are all within 5%. This is hardly surprising as the layout of the prototype is balanced, that is, as shown in Fig. 9(a) and (b), the position and distances between conductors in XOZ and YO(O′)Z sections are the same and the insulating mediums between the conductors are uniform. As a result, the capacitive effects of the left-XOZ and YO′Z section are almost the same, so are the right-XOZ and YOZ section. For most all-insulation transformers with racetrack windings, the conductors and

TABLE III
CAPACITANCE PARAMETERS OF THE TRANSFORMER (PF)

Equation	C_{12}	C_{34}	C_{24}	C_{13}	C_{23}	C_{14}	C_{10}	C_{20}	C_{30}	C_{40}
(7)	8.1	14.2	97.5	100.2	60.2	58.9	166.3	165.8	34.2	31.1
(9)	8.3	13.9	93.0	95.5	61.7	59.1	161.1	160.6	35.3	29.9
RE (%)	2.5	−2.1	−4.6	−4.7	2.5	0.3	−3.1	−3.1	3.2	−3.9

insulation mediums may be taken as balanced layout. In this case, only one axial section of the transformer is needed to be calculated to extract capacitance parameters, and computation cost will be further reduced in engineering application.

IV. EXPERIMENTAL VERIFICATION OF THE MODEL

To verify that the proposed wideband mechanism model and its parameter extraction method are effective for the H^{3}Ts, impedance characteristics of the prototype under open circuit, short circuit, and load (a 125 kΩ resistance load and a 40-μH inductance load) conditions are measured by an Agilent 4294A impedance analyzer, frequency ranging from 100 Hz to 1 MHz. Careful compensations of connecting cables are conducted to improve the accuracy of experimental results, and impedance curves are acquired repeatedly with different supply current levels of impedance analyzer to ensure the prototype working linearly [20]. The measurements are conducted on both sides of the prototype. For convenience, subscript "1" and "2" of the impedances represent that the impedance analyzer is connected to the LV winding and HV winding, and "OC," "SC," "R," and "L" represent that another winding is open circuit, short circuit, load with a resistance and load with an inductance, respectively.

Fig. 11 shows the measurement and simulation results under open- and short-circuit conditions, and Fig. 12 shows the measurement and simulation results under load conditions. In Figs. 11 and 12, the solid lines indicate results measured by the impedance analyzer and the dash lines indicate results calculated by a circuit simulator based on the proposed wideband mechanism model. A good agreement between the measurement and simulation results may be observed with the frequency nearly up to 300 kHz. The results indicate that the proposed model represents the magnetic and electrostatic couplings of the H^{3}T accurately. Meanwhile, the validity of parameter extraction methods proposed in Section III is also verified. It should be noted that 300 kHz is not an inherent frequency limit of the proposed model. Actually, for another H^{3}T prototype with different values for its geometric parameters or different materials used, effective frequency range of the proposed model may be changed due to different magnetic and capacitive parameters of the transformer.

V. DISCUSSIONS

For isolated dc–dc converters based on modular multilevel converter, the HF transformers may provide galvanic isolation of the system to achieve separate grounding arrangements between two HVDC networks, and no winding of the H^{3}T has to be grounded [2], [3]. However, for certain dc–dc converters with specific topologies, such as an isolated dual-channel quasi resonant dc–dc converter, winding of the transformer may have to be grounded to avoid the midpoint floated [27]. Different with a traditional low-power HF transformer whose magnetic core is made of ferrite and insulated, the metallic core of the H^{3}T is a conductor and has to be grounded to avoid partial discharges. Therefore, electrical links will be formed between the magnetic core and the winding which is grounded, and capacitive effects of the H^{3}T may be changed. Accordingly, it is necessary to discuss the feasibility of the proposed model under different winding grounding conditions. Furthermore, in these cases, the relationships between the proposed model and traditional six and three capacitance models are also revealed in this section.

A. Theoretical Analysis Based on Capacitance Matrix

Based on the potential of each electrode φ_i, the charges stored on each electrode Q_i may be represented as

$$\{Q_i\} = [C]\{\varphi_i\}, i = 1, 2, 3, 4 \tag{10}$$

where $[C]$ is capacitance matrix of the proposed model

$$\begin{bmatrix} \sum_{i=0,i\neq 1}^{4} C_{1i} & -C_{12} & -C_{13} & -C_{14} \\ -C_{21} & \sum_{i=0,i\neq 2}^{4} C_{2i} & -C_{23} & -C_{24} \\ -C_{31} & -C_{32} & \sum_{i=0,i\neq 3}^{4} C_{3i} & -C_{34} \\ -C_{41} & -C_{42} & -C_{43} & \sum_{i=0,i\neq 4}^{4} C_{4i} \end{bmatrix}.$$

Considering that these capacitances are sufficient to characterize all capacitive couplings of the H^{3}T from external-behavior perspective, grounding of the transformer windings may cause changes of capacitance matrix as follows.

If the primary winding is grounded, electrode 2 will be merged into the ground (electrode 0) and a "contraction" may be occurred in the capacitance matrix [28]. That is, the second row and column of $[C]$ will be removed. The equivalent model is shown in Fig. 13(a) and $[C]$ will be reduced to

$$\begin{bmatrix} \sum_{i=0,i\neq 1}^{4} C_{1i} & -C_{13} & -C_{14} \\ -C_{31} & \sum_{i=0,i\neq 3}^{4} C_{3i} & -C_{34} \\ -C_{41} & -C_{43} & \sum_{i=0,i\neq 4}^{4} C_{4i} \end{bmatrix}.$$

Similarly, if the secondary winding is grounded, electrode 4 will be merged into the ground. The equivalent model is shown

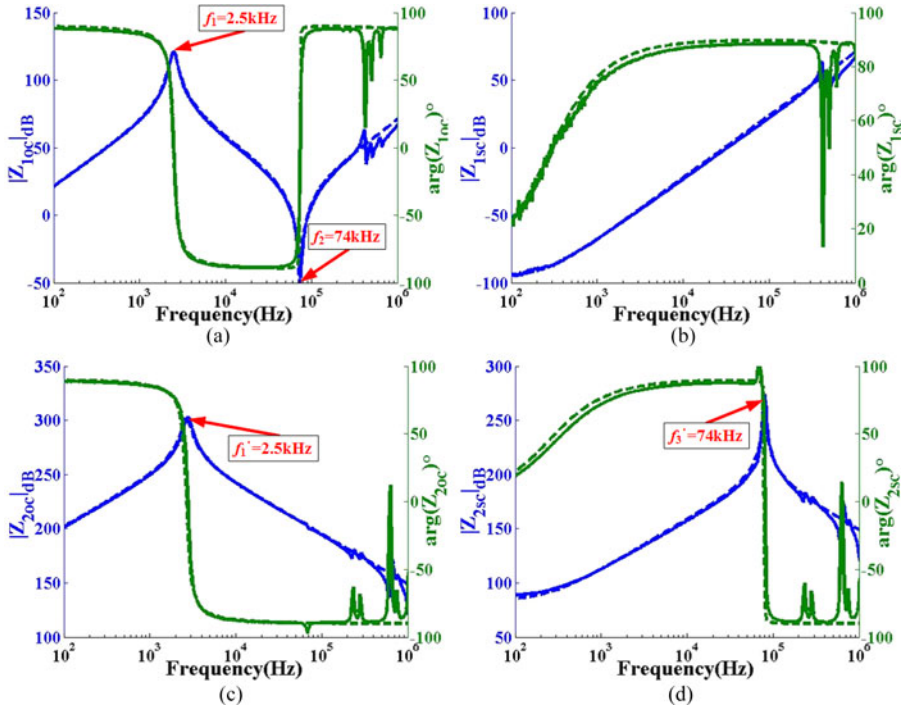

Fig. 11. Modules and phases of impedances for open and short circuit: measured (solid lines) and simulated based on the wideband mechanism model (dash lines). (a) HV winding is open circuit. (b) HV winding is short circuit. (c) LV winding is open-circuit. (d) LV winding is short circuit.

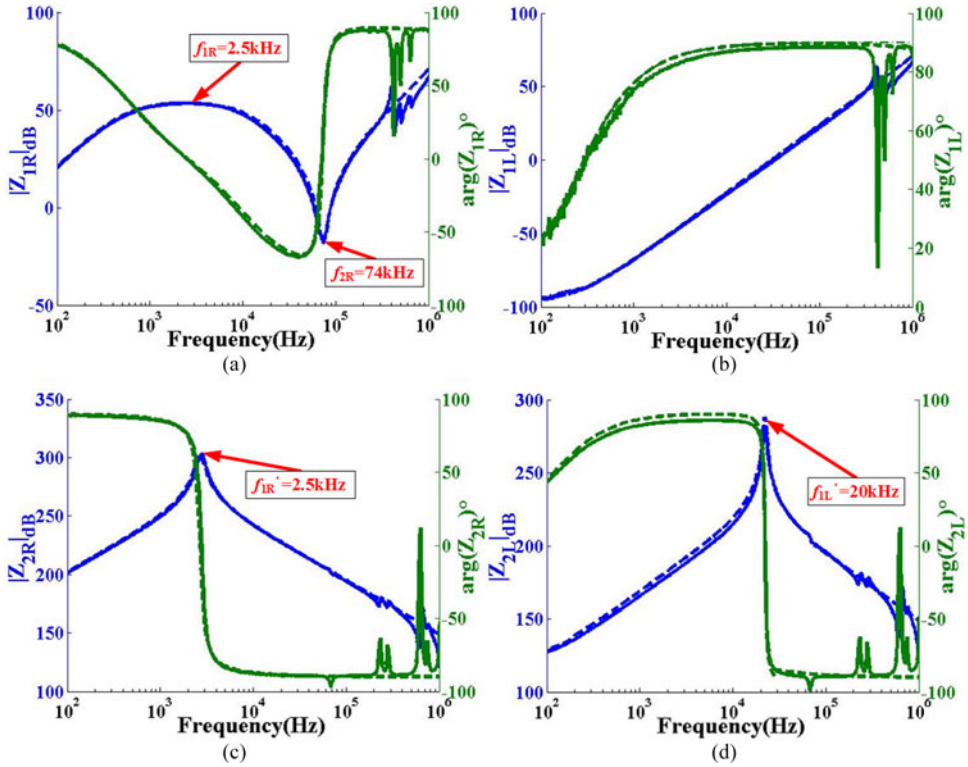

Fig. 12. Modules and phases of impedances for a resistive load and an inductive load: measured (solid lines) and simulated based on the wideband mechanism model (dash lines). (a) HV winding load with a resistance. (b) HV winding load with an inductance. (c) LV winding load with a resistance. (d) LV winding load with an inductance.

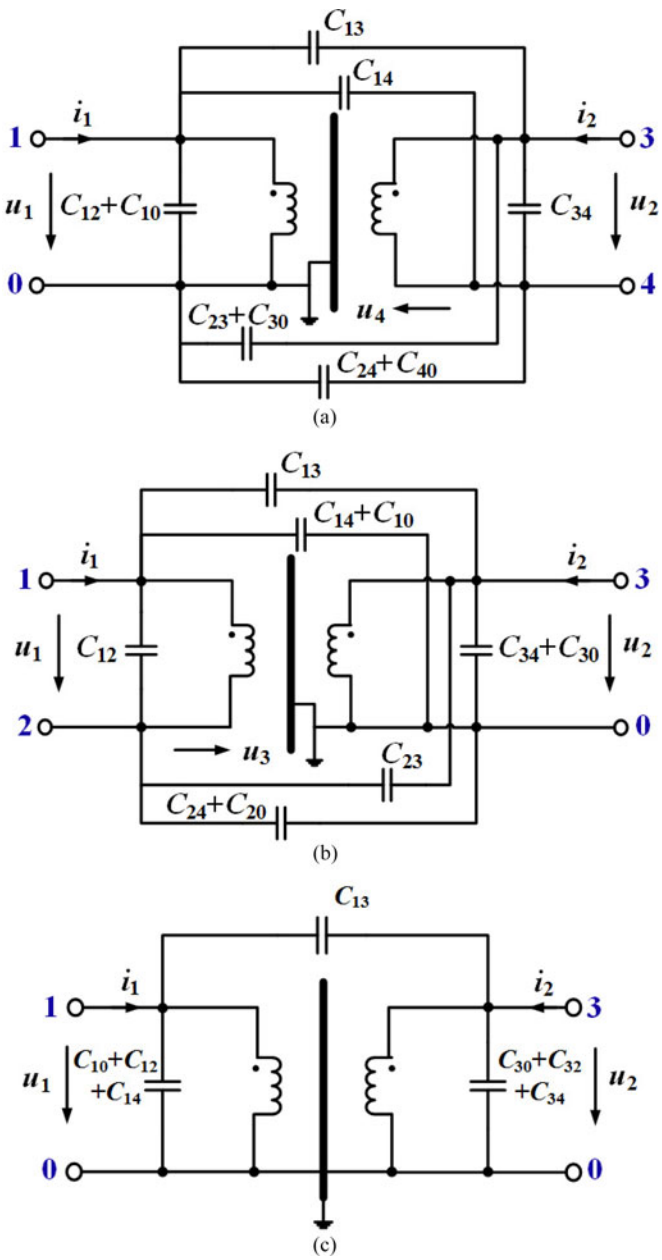

Fig. 13. Equivalent circuits of the proposed capacitive model under different winding conditions. (a) LV winding is grounded. (b) HV winding is grounded. (c) LV and HV winding are both grounded.

in Fig. 13(b) and $[C]$ will be reduced to

$$\begin{bmatrix} \sum_{i=0,i\neq 1}^{4} C_{1i} & -C_{13} & -C_{13} \\ -C_{21} & \sum_{i=0,i\neq 2}^{4} C_{2i} & -C_{23} \\ -C_{31} & -C_{32} & \sum_{i=0,i\neq 3}^{4} C_{3i} \end{bmatrix}.$$

If the primary and secondary windings are both grounded, electrodes 2 and 4 will be merged into the ground. The equivalent model is shown in Fig. 13(c) and $[C]$ will be reduced to

$$\begin{bmatrix} \sum_{i=0,i\neq 1}^{4} C_{1i} & -C_{13} \\ -C_{31} & \sum_{i=0,i\neq 3}^{4} C_{3i} \end{bmatrix}.$$

Based on the above analysis, it may be found that the grounding of windings in the H^{3}T will change capacitive effects of the transformer as the order of capacitance matrix is reduced. Specifically, when the LV winding is grounded, the proposed capacitive mechanism model is reduced to a well-known six-capacitance model as the grounding magnetic core is referred to the LV side and the LV-winding-to-ground capacitance, i.e., C_{20} in this case, is shorted as shown in Fig. 13(a). Similarly, when the HV winding is grounded, the proposed model is reduced to another six-capacitance model as the HV-winding-to-ground capacitance, i.e., C_{40} in this case, is shorted as shown in Fig. 13(b). When the LV and HV winding are both grounded, the proposed model is reduced to a traditional three-capacitance model as the capacitances of the LV and HV winding to the ground as well as one capacitance between the LV and HV windings, i.e., C_{20}, C_{40}, and C_{24}, are all shorted as shown in Fig. 13(c).

B. Experimental Verification

To verify the validity of the proposed capacitive model when the winding is grounded and corresponding analysis based on the capacitance matrix, the impedance characteristics of the prototype under different winding grounding conditions are measured, and corresponding simulations are conducted with the equivalent circuits of the proposed model as shown in Fig. 13. The measurement and simulation results of open-circuit impedances seen from the LV side of the prototype when the LV winding is grounded, the HV winding is grounded and the two windings are both grounded are shown in Fig. 14(a), (b), and (c), respectively, where the solid lines indicate the results measured by the impedance analyzer and the dash lines indicate the results calculated by a circuit simulator based on the equivalent circuits. A good agreement between the measurement and simulation results may be observed in Fig. 14. Actually, the open- and short-circuit impedances of the prototype seen from both sides under different winding grounding conditions are all measured and simulated. The results are also in good agreement, but not presented here due to limited space. The results shown in Fig. 14 are representative and typical due to their abundant information on resonances.

The experimental and simulated results indicate that the proposed mechanism model is valid in different grounding cases, including all winding floated, one of the LV or HV winding grounded and both the two windings grounded. Furthermore, it is proved that the proposed capacitive model will be reduced to traditional six or three capacitance model when one or two windings of the transformer are grounded as the proposed model has a more complete capacitance matrix.

TABLE IV
RESONANT FREQUENCIES UNDER DIFFERENT GROUNDING CONDITIONS (KHZ)

Resonant Frequency	No winding Grounded	LV winding Grounded	HV winding Grounded	Both windings Grounded
f_1	2.5	2.5	2	1.8
f_2	74	74	60	53

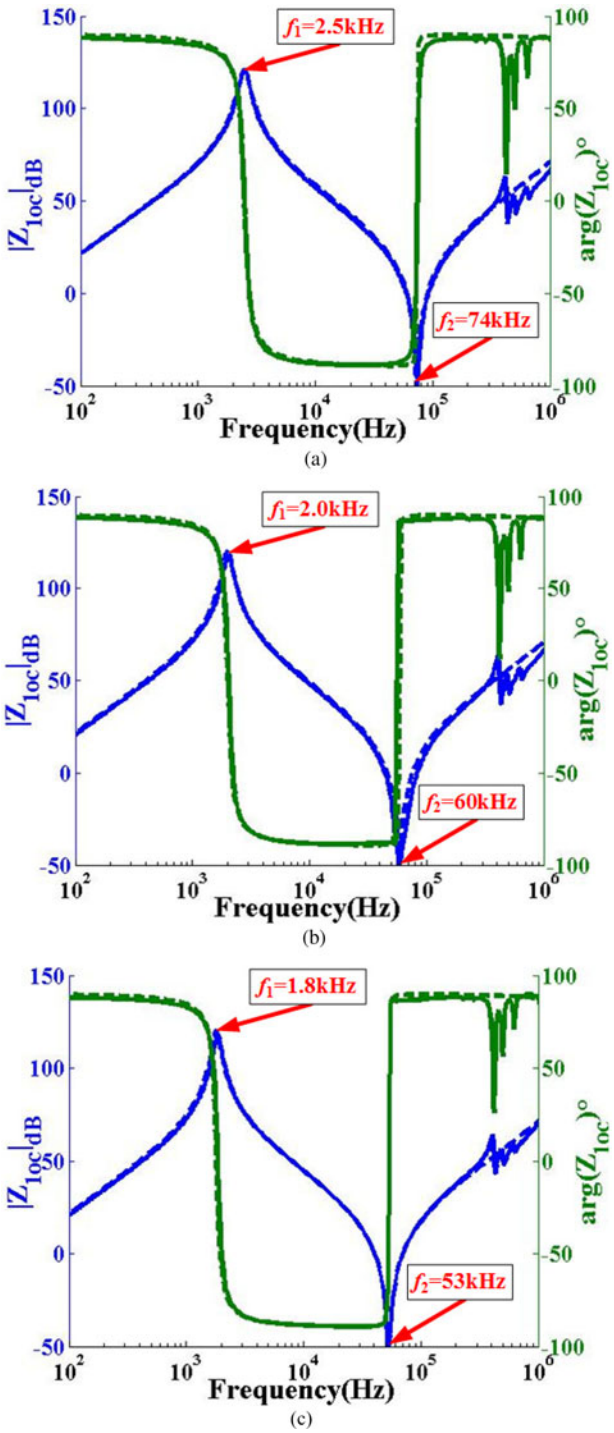

Fig. 14. Modules and phases of open-circuit impedances seen from the LV winding under different winding grounding conditions: measured (solid lines) and simulated (dash lines). (a) LV winding is grounded. (b) HV winding is grounded. (c) LV and HV winding are both grounded.

C. Impacts of Winding-to-Ground Capacitances on Resonant Frequencies

The resonant frequencies of the open-circuit impedance characteristics seen from the LV side under different winding grounding conditions are shown in Table IV. Compared with the situation that no winding is grounded, when the LV winding is grounded the resonant frequencies remain unchanged. However, when the HV winding is grounded and the two windings are both grounded, significant shifts of the resonant frequencies are observed. This phenomenon, which is hard to be explained using traditional six or three capacitance models, may be accounted for by the proposed wideband mechanism model. Comparing values of the LV-winding-to-ground capacitances and the HV-winding-to-ground capacitances referred to the primary side, i.e., C_{10}, C_{20}, and n^2C_{30}, n^2C_{40} (161.1, 160.6 pF and 295.9, 249.2 nF), it may be found that as the LV winding only has 12 turns, C_{10} and C_{20} are very small and may have little impact on impedance characteristics of the transformer. However, the HV winding has 1096 turns and n^2C_{30}, n^2C_{40} may not be ignored. As a result, grounding of the HV winding will cause resonant frequencies shift as C_{40} is shorted. When the two windings are both grounded, besides C_{20} and C_{40}, one capacitance between the two windings, i.e., C_{24} is also shorted, which causes the resonant frequencies to shift further.

In summary, the proposed wideband mechanism model is effective to explain the impacts of grounding windings on resonant frequencies of the H^{3}T by analyzing the effects of winding-to-ground capacitances. Furthermore, for an H^{3}T in the design phase, external behaviors of the transformer, including natural resonances, transmission characteristic, etc., may be also predicted and adjusted by evaluating parameters of the proposed model through electromagnetic computation based on geometry of the transformer, no matter windings of the transformer are floated or grounded. Corresponding studies will be conducted and developed in the future.

VI. CONCLUSION

A wideband mechanism model and its parameter extraction method for the H^{3}T are proposed in this paper. The impedance characteristics of an H^{3}T prototype are measured under open circuit, short circuit, and load conditions to verify the proposed model and the parameter extraction method. In addition, when different windings of the H^{3}T are grounded, validity of the proposed model and its relationships with traditional models are discussed and verified. The results show that:

1) With elaborate considerations on magnetic and capacitive effects of the H^{3}T, including the electrostatic couplings between windings, magnetic core and enclosure of the

transformer, the proposed mechanism model is sufficient to characterize the wideband impedance characteristics of the H^3T, and the valid frequency band is up to 300 kHz for the prototype evaluated in this paper.

2) Considering large number of winding turns and racetrack windings of the H^3T, the 2-D FEM based on weighted algorithm proposed in this paper is effective and convenient to extract capacitance parameters. Furthermore, for a balanced layout H^3T where positions and distances between conductors in different axial sections are the same and insulating mediums between the conductors are uniform, it may be feasible to calculate only one axial section of the transformer.
3) When the LV or HV winding is grounded, or the two windings are both grounded, the proposed model will be reduced to traditional six or three capacitance models as corresponding winding-to-ground capacitances are shorted, which may account for the shift of transformer resonant frequencies. The proposed wideband mechanism model and corresponding parameter extraction method are helpful to electromagnetic design and external behavior investigations of the H^3T.

REFERENCES

[1] A. A. Hagar and P. W. Lehn, "Comparative evaluation of a new family of transformerless modular DC-DC converters for high-power applications," *IEEE Trans. Power Electron.*, vol. 29, no. 1, pp. 444–452, Oct. 2014.

[2] S. Kenzelmann, A. Rufer, D. Dujic, F. Canales and Y. R. de Novaes, "Isolated DC/DC structure based on modular multilevel converter," *IEEE Trans. Power Electron.*, vol. 30, no. 1, pp. 89–98, Jan. 2015.

[3] T. Luth, M. M. C. Merlin, T. C. Green, F. Hassan, and C. D. Barker, "High-frequency operation of a DC/AC.DC system for HVDC applications," *IEEE Trans. Power Electron.*, vol. 29, no. 8, pp. 4107–4115, Aug. 2014.

[4] G. Ortiz, J. Biela, D. Bortis, and J. W. Kolar, "1 Megawatt, 20 kHz, isolated, bidirectional 12kV to 1.2kV DC-DC converter for renewable energy applications," in *Proc. Int. Power Electron. Conf.*, Jun. 21–24, 2010, pp. 3212–3219.

[5] W. Shen, F. Wang, D. Boroyevich, and C. W. Tipton IV, "High-density nanocrystalline core transformer for high-power high-frequency resonant converter," *IEEE Trans. Ind. Appl.*, vol. 44, no. 1, pp. 213–222, Jan./Feb. 2008.

[6] Y. Du, S. Baek, S. Bhhattacharya, and A. Q. Huang, "High-voltage high-frequency transformer design for a 7.2kV to 120V/240V 20kVA solid state transformer," in *Proc. IEEE 36th Annu. Conf. Ind. Electron. Soc.*, Nov. 2010, pp. 493–498.

[7] Y. A. Wang and D. M. Xiao, "Prototype design for a high-voltage high-frequency rectifier transformer for high power use," *IET Power Electron.*, vol. 4, no. 6, pp. 615–623, Feb. 2010.

[8] H. Fan and H. Li, "High-frequency transformer isolated bidirectional DC-DC converter modules with high efficiency over wide load range for 20kVA solid-state transformer," *IEEE Trans. Power Electron.*, vol. 26, no. 12, pp. 3599–3608, Dec. 2011.

[9] A. Garcia-Bediaga, U. Viscarret, I. Etxeberria-Otadui, and A. Rufer, "Proposal and validation of medium-frequency power transformer design methodology," in *Proc. IEEE Energy Convers. Congr.. Expo.*, Sep. 17–22, 2011, pp. 3792–3799.

[10] H. Lu, J. Zhu, and S. Y. Ron Hui, "Experimental determination of stray capacitances in high frequency transformers," *IEEE Trans. Power Electron.*, vol. 18, no. 5, pp. 1105–1112, Sep. 2003.

[11] J. Biela and W. Johann, "Using transformer parasitics for resonant converters-A review of the calculation of the stray capacitance of transformers," *IEEE Trans. Ind. Appl.*, vol. 44, no. 1, pp. 223–233, Jan./Feb. 2008.

[12] X. Margueron and J. P. Keradec, "Identifying the magnetic part of the equivalent circuit of n-winding transformers," *IEEE Trans. Instrum. Meas.*, vol. 56, no. 1, pp. 146–152, Feb. 2007.

[13] W. M. Colonel and T. Mclyman, *Transformer and Inductor Design Handbook*, 3rd ed. Boca Raton, FL, USA: CRC Press, 2004.

[14] Z. De Grève, O. Deblecker, and J. Lobry, "Fast computation of R, L parameters of high frequency multi-winding magnetic components," *Int. J. Comput. Math. Elect. Electron. Eng.*, vol. 30, no. 6, pp. 1914–1926, 2011.

[15] J. Liu, X. Cui, Z. Fei, and H. Shao, "3D non-linear anisotropic magnetostatic field computation in reactor," *COMPEL*, vol. 17, nos. 1–3, pp. 239–243, 1998.

[16] J. Yuan, N. Chen, W. Li, X. Cui, and H. Shao, "The calculation of short-circuit reactance of transformers by complementary variational principles," *IEEE Trans. Magn.*, vol. 28, no. 2, pp. 1422–1425, Mar. 1992.

[17] F. De Leon and A. Semlyen "Time domain modelling of eddy currents for transformer transients," *IEEE Trans. Power Del.*, vol. 8, no. 1, pp. 271–280, Jan. 1993.

[18] F. de Leon and A. Semlyen, "Efficient calculation of elementary parameters of transformers," *IEEE Trans. Power Electron.*, vol. 7, no. 1, pp. 376–383, Jan. 1992.

[19] M. M. Kane and S. V. Kulkarni, "MTL-based analysis to distinguish high-frequency behavior of interleaved windings in power transformers," *IEEE Trans. Power Del.*, vol. 28, no. 4, pp. 2291–2299, Oct. 2013.

[20] B. Cogitore, J. P. Keradec, and J. Barbaroux, "The two-winding transformer: An experimental method to obtain a wide frequency range equivalent circuit," *IEEE Trans. Instrum. Meas.*, vol. 43, no. 2, pp. 364–371, Apr. 1994.

[21] A. Schellmanns, J.-P. Keradec, J.-L. Schanen, and K. Berrouche, "Representing electrical behavior of transformers by lumped element circuits: as global physical approach," in *Proc. IEEE 34th IAS Annu. Meeting Conf. Rec. Ind. Appl. Conf.*, 1999, vol. 3, pp. 2100–2107.

[22] Z. De Grève, O. Deblecker, and J. Lobry, "Numerical modeling of capacitive effects in HF multiwinding transformers—Part I: A rigorous formalism based on the electrostatic equations," *IEEE Trans. Magn.*, vol. 49, no. 5, pp. 2017–2020, May 2013.

[23] Z. De Grève, O. Deblecker, and J. Lobry, "Numerical modeling of capacitive effects in HF multiwinding transformers—Part: Identification using the finite-element method," *IEEE Trans. Magn.*, vol. 49, no. 5, pp. 2021–2024, May 2013.

[24] R. Asensi, R. Prieto, J. A. Cobos, and J. Uceda, "Modeling high-frequency multiwinding magnetic components using finite-element analysis," *IEEE Trans. Magn.*, vol. 43, no. 10, pp. 3840–3850, Oct. 2007.

[25] Y. Yoshizawa, S. Oguma, and K. Yamaguchi, "New Fe-based soft magnetic alloys composed of ultrafine grain structure," *J. Appl. Phys.*, vol. 64, pp. 6044–6046, 1988.

[26] G. Antonini, A. Orlandim, and C. R. Paul, "Internal impedance of conductors of rectangular cross section," *IEEE Trans. Microw. Theory Tech.*, vol. 47, no. 7, pp. 979–985, Jul. 1999.

[27] J. Hamar, I. Nagy, P. Stumpf, H. Ohsaki, and E. Masada, "New dual channel quasi resonant DC-DC converter topologies for distributed energy utilization," in *Proc. 13th Power Electron. Motion Control Conf.*, 2008, pp. 1778–1785.

[28] N. Balabanian and T. A. Bickart, *Electrical Network Theory*. New York, NY, USA: Wiley, 1969.

Chen Liu was born in Shandong, China, in 1990. He received the B.Sc. degree in electrical engineering from North China Electric Power University, Beijing, China, in 2012, where he is currently working toward the Ph.D. degree.

His research interests include advanced transmission technology in power systems and electromagnetic modeling of high power high frequency transformer for HVDC application.

Lei Qi was born in Henan, China, in 1978. He received the B.S., M.S., and Ph.D. degrees in electrical engineering from North China Electric Power University, Baoding, China, in 2000, 2003, and 2006, respectively.

He is currently an Associate Professor of electrical and electronic engineering at North China Electric Power University, Beijing, China. His research interests include electromagnetic (EM) field numerical computation, EM compatibility on power systems, and ultrahigh-voltage power transmission technology.

Xiang Cui (M'97–SM'98) was born in Baoding, Hebei, China, in 1960. He received the B.Sc. and M.Sc. degrees in electrical engineering from North China Electric Power University, Baoding, China, in 1982 and 1984, respectively, and the Ph.D. degree in accelerator physics from China Institute of Atomic Energy, Beijing, China, in 1988.

He is currently a Professor and the Head of the Electromagnetic Fields and Electromagnetic Compatibility Laboratory, North China Electric Power University. His research interests include computational electromagnetics, electromagnetic environment and electromagnetic compatibility in power systems, insulation, and magnetic problems in high-voltage apparatus.

Prof. Cui is a Standing Council Member of the China Electrotechnical Society, a Fellow of the Institution of Engineering and Technology, a Member of CIGRE C4.02.01 Working Group (electromagnetic compatibility in power systems). He is also an Associate Editor of the IEEE TRANSACTIONS ON ELECTROMAGNETIC COMPATIBILITY and a Member of the Editorial Advisory Board of the INTERNATIONAL JOURNAL FOR COMPUTATION AND MATHEMATICS in electrical and electronic engineering.

Zhiyuan Shen received the B.Sc. degree in electrical engineering in North China Electric Power University, Beijing, China, in 2014, where he is currently working toward the M.Sc. degree.

His main research interests include HVDC Flexible, dc/dc converters, and IGBT testing and modeling.

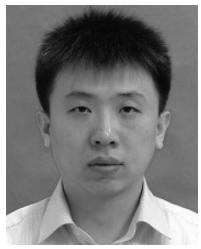

Xiaoguang Wei received the bachelor's of engineering and master's of engineering degrees from North China Electric Power University, Beijing, China, in 1999 and 2003, respectively. He received the Ph.D. degree in engineering from China Electric Power Research Institute, Nuremberg, Germany, in 2007.

He is currently with State Grid Smart Research Institute, DC Transmission Technology Research Department, Beijing. His research interests include HVDC transmission, dc power grid and its key equipment research and development, and the connection of new energy to power grid.